Distortion-free enhancement of terahertz signals measured by electro-optic sampling. II. Experiment

**Jeremy A. Johnson,[1,*] Fabian D. J. Brunner,[2] Sebastian Grübel,[1] Andrés Ferrer,[3]
Steven L. Johnson,[3] and Thomas Feurer[2]**

[1]FEMTO Group, Swiss Light Source, Paul Scherrer Institute, 5323 Villigen, Switzerland
[2]Institute of Applied Physics, University of Bern, 3012 Bern, Switzerland
[3]Institute of Quantum Electronics, ETH Zurich, 8093 Zurich, Switzerland
*Corresponding author: jeremy.johnson@psi.ch

Three methods for distortion-free enhancement of electro-optic sampling measurements of terahertz signals are tested. In the first part of this two-paper series [J. Opt. Soc. Am B **31**, 904–910 (2014)], the theoretical framework for describing the signal enhancement was presented and discussed. As the applied optical bias is decreased, individual signal traces become enhanced but distorted. Here we experimentally show that nonlinear signal components that distort the terahertz electric field measurement can be removed by subtracting traces recorded with opposite optical bias values. In all three methods tested, we observe up to an order of magnitude increase in distortion-free signal enhancement, in agreement with the theory, making possible measurements of small terahertz-induced transient birefringence signals with increased signal-to-noise ratio.   © 2014 Optical Society of America

OCIS codes: (260.1440) Birefringence; (040.2235) Far infrared or terahertz; (300.6495) Spectroscopy, terahertz.

http://dx.doi.org/10.1364/JOSAB.31.001035

1. INTRODUCTION

Terahertz time-domain spectroscopy has become an important tool in scientific research as well as in industry. In order to quantify optical properties of materials in the terahertz frequency regime or to study terahertz-radiation-induced dynamics, accurate measurements of the terahertz electric field and a high signal-to-noise ratio are essential. A common method of measuring the terahertz electric field is free-space electro-optic (EO) sampling in crystals such as ZnTe or GaP [1,2]. EO sampling requires a simple transient birefringence setup where the terahertz electric field induces a change in ellipticity to an optical probe pulse while propagating through the EO crystal [3,4]. In such a transient birefringence setup, if one simply has crossed ideal polarizers P1 and P2 placed before and after the EO crystal with a photodetector after each channel of the analyzer P2, in the absence of birefringence in the EO crystal all light reaches one detector and no light reaches the other; inserting a $\lambda/4$ wave plate (QWP) or other polarization optic such as a compensator or variable wave plate (VWP) creates optical bias and can balance the detectors placed in each channel of the polarizing beam splitter in the conventional EO sampling scheme. The intensity in each channel of the polarizing beam splitter is monitored, often using balanced photodiodes, and the terahertz-field-induced signal is recorded as the difference in the two channels as a function of pump-probe delay. Under many experimental conditions, this signal is directly proportional to the electric field, and using the relative signal modulation and the appropriate EO crystal material properties, one can extract the absolute electric field amplitude as a function of time [5,6].

A common technique with a nearly identical experimental setup is optically heterodyne-detected optical Kerr effect spectroscopy (OHD-OKE) [7–9]. In the first of this two-paper series [10], we showed that under the condition of low optical bias and small signals, EO sampling can be thought of as a heterodyned transient birefringence measurement; and we showed that as some of the methodology of OHD-OKE measurements is adopted, namely working with small optical bias and correcting for signal distortions by recording data with opposite optical biases, large enhancements to terahertz-induced transient birefringence signals are expected. Here we test the theory and show that in practice we can achieve EO signal enhancements of one order of magnitude without distortions in the time-domain electric field.

2. EXPERIMENTAL SETUP

The relevant optics to monitor the transient birefringence include an initial polarizer (P1), a QWP or VWP, the EO crystal, and a final analyzer (P2). In Fig. 1 we show a schematic of the experimental setup we use here. Terahertz radiation, generated by optical rectification in the organic crystal OH1 [11,12], is focused with an off-axis parabolic mirror to the EO crystal [300 μm (110)-cut GaP] with the terahertz polarized along [$\bar{1}$10]. An 800 nm wavelength probe light derived from a Ti:sapphire amplifier is directed through a high-quality polarizer (P1), then to either a QWP or VWP. Note that here we insert the QWP or VWP before the EO crystal [10] rather than after as is common practice. The probe beam is focused with a lens (L1) through a hole in the parabolic mirror to the EO crystal, then collimated with another lens after the EO crystal (L2), and a Wollaston prism (P2) splits perpendicular polarizations,
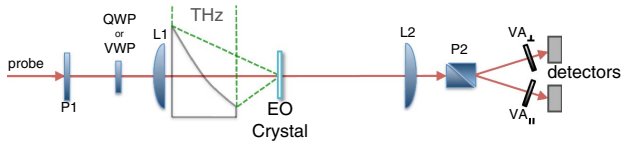
Fig. 1. Schematic of the transient birefringence setup. A high-quality polarizer P1 sets the probe polarization. Optical bias is applied by either using a variable wave plate (VWP) or a QWP after P1. Either the VWP, the QWP, or P1 can be rotated to vary the level of optical bias, as described in the text. Another high-quality polarizer (P2) serves as analyzer, here depicted as a Wollaston prism as in the current measurements. Lens L1 focuses the probe beam to the EO crystal, and L2 collimates it after. Detectors monitor the perpendicular and parallel channels, each of which has a variable attenuator (VA). An off-axis parabolic mirror focuses the terahertz to the EO crystal or the sample, collinearly with the probe beam.

which are directed to individual photodiodes. In our experimental setup, a variable attenuator (VA) was placed in each of the polarization channels for independently adjusting the light levels on the photodiodes. Using the usual EO sampling scheme and appropriate coefficients for the GaP crystal [3,5,6], the generated peak electric field was approximately 100 kV/cm for all measurements.

As described in the following, we will vary the positioning of the polarization optics, and thus the orientations are defined as follows. A zero degree orientation of P1 ($\phi = 0°$) is defined such that vertically polarized light is transmitted. The Wollaston prism P2 is set such that in the absence of other optics there is minimum transmission in the perpendicular (horizontally polarized) channel. At 0° the QWP is oriented such that the fast optical axis is vertical ($\theta = 0°$). The compensator is set at 45° from the P1 polarization. The EO crystal is set so the [$\bar{1}$10] GaP direction is vertical and parallel to the terahertz polarization, as well as initially vertically polarized probe light. Alternatively, the GaP crystal and terahertz polarization could be rotated 90° for an equivalent EO birefringence signal. Due to the use of real optics, which may have some strain-induced birefringence, these angles were adjusted slightly as recommended in the OHD-OKE literature [9]; P1 was set to 0°, then the angles of the QWP or VWP and P2 were iteratively adjusted to minimize the transmission in the perpendicular Wollaston channel. Typically for high-quality optical elements this is only a small adjustment from the nominal zero values. It is important to point out that due to the extreme sensitivity to the polarization state of the probe beam with this detection technique, optical elements that can potentially alter the probe polarization should be kept at a minimum or removed from the optical path between P1 and P2. Dielectric mirrors in particular may significantly alter the polarization state for beams with polarization not purely s or p. In the current measurements, the only optical elements placed between polarizers P1 and P2 were those displayed in Fig. 1: the QWP or VWP, two lenses, and the EO crystal. The quality of the polarizers and the optical elements between them determines the level of scattered light and therefore, as described in Ref. [10], affects the maximum signal enhancement that can be achieved at low optical bias.

Physically, the optical bias level corresponds to the set angles of the polarization optics. In a commonly used EO sampling configuration, P1 is set to $\phi = 0°$ and a QWP is oriented at $\theta = 45°$; this gives an optical bias of 90°. As reported below, a large signal enhancement is seen as the optical bias is

reduced from the typical EO sampling case to small angles as in OHD-OKE measurements. In the three cases considered, the optical bias is changed by (1) rotating P1 to a given angle ϕ and keeping a QWP fixed at $\theta = 0°$, (2) keeping P1 fixed at $\phi = 0°$ and rotating the QWP to a given angle θ, and (3) keeping P1 stationary and adjusting the phase retardation of a VWP. As described in the theoretical paper [10], mathematically case 1 and case 3 give identical results.

To monitor the light intensity in perpendicular and parallel channels from the Wollaston prism, we recorded the signal simultaneously from two separate photodiodes with the output connected to gated integrators and a data acquisition card/PC data acquisition system [13]. The pump beam was chopped at half the 1 kHz repetition rate, and the normalized and balanced difference signal was recorded as

$$S(E_{THz}, \Gamma_0) = \frac{T_\perp I_\perp(E_{THz}, \Gamma_0) - T_\parallel I_\parallel(E_{THz}, \Gamma_0)}{T_\perp I_\perp(0, \Gamma_0) + T_\parallel I_\parallel(0, \Gamma_0)}, \quad (1)$$

where E_{THz} is the terahertz electric field for a given pump/probe delay and Γ_0 is the optical bias. The intensities with zero electric field in the denominator are recorded when the terahertz pump is blocked by the chopper, the intensities in the numerator are recorded when the terahertz pump is unblocked, and the attenuation factors $T_\perp$ and $T_\parallel$ are set by the variable attenuators $VA_\perp$ and $VA_\parallel$ before each photodiode. In order to maintain similar detector-induced noise levels in all traces, for the lowest optical bias setting the maximum intensity for the perpendicular channel was measured ($T_\perp = 1$), and $T_\parallel$ was set to equalize the light level in both detectors. For subsequent measurements with increasing optical bias (and therefore increasing intensity in the perpendicular channel), $T_\perp$ was reduced to maintain the original intensity level and $T_\parallel$ was adjusted to balance the diodes, so that in the absence of an electric field, the difference signal was zero and the light level on both photodiodes was identical for all measurements. Note that in Ref. [10], $T_\perp$ is 1 and $T_\parallel$ is adjusted to obtain balanced detection when no terahertz is present.

3. RESULTS AND DISCUSSION

For case 1 (rotating P1 and keeping the QWP fixed at 0°), traces were recorded for $\phi = \pm 1°$, $\pm 2°$, $\pm 5°$, $\pm 10°$, $\pm 20°$, $\pm 30°$, and $\pm 45°$ corresponding to optical biases of $\Gamma_0 = \pm 2°$, $\pm 4°$, $\pm 10°$, $\pm 20°$, $\pm 40°$, $\pm 60°$, and $\pm 90°$. For case 2 (P1 at $\phi = 0°$ and rotating the QWP), traces were recorded for $\theta = \pm 1°$, $\pm 2°$, $\pm 5°$, $\pm 10°$, $\pm 20°$, $\pm 30°$, and $\pm 45°$ corresponding to optical biases of $\Gamma_0 = \pm 2°$, $\pm 4°$, $\pm 10°$, $\pm 21°$, $\pm 48°$, $\pm 74°$, and $\pm 90°$. For case 3 (P1 at $\phi = 0°$ and adjusting the VWP), traces were recorded for optical biases of $\Gamma_0 = \pm 5.9°$, $\pm 10°$, $\pm 14.6°$, $\pm 26°$, $\pm 40°$, $\pm 58°$, and $\pm 80°$. In all three cases, the optical bias was calculated in the approximation of zero strain-induced birefringence [10], and experimentally, the positive angles were set with $\pm 0.1°$ precision and the negative optical-bias magnitude was set by making the intensity in the perpendicular P2 channel equal to the intensity level of the positive optical bias.

Traces collected utilizing case 1 (rotating P1) are displayed in Fig. 2; in Fig. 2(a) we see traces collected for decreasing positive optical bias, and Fig. 2(b) shows traces recorded
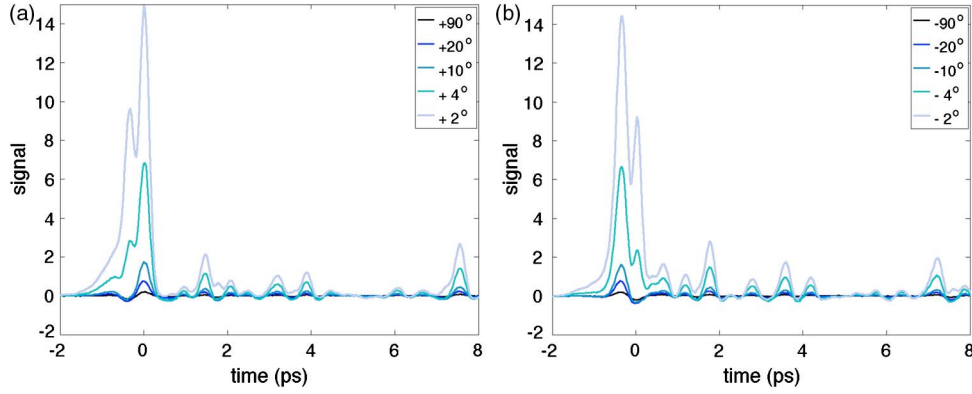
Fig. 2. Terahertz-induced EO transient birefringence data collected for different P1 angles with QWP fixed at 0°. (a) The normalized difference signal for positive optical biases corresponding to $\Gamma_0 = 2\phi$ shown in the key. (b) The normalized difference signal for negative optical biases shown in the key.

for decreasing negative bias magnitude. Optical bias magnitudes of 40° and 60° were omitted because they are nearly identical to the 90° traces. For both positive and negative optical bias, an increasing positive signal is observed as the optical bias magnitude is reduced. Due to the large signal increase above the 90° optical bias conditions, care needs to be taken to ensure that the detection components are not saturated for the largest signal.

In the optical heterodyne detection framework (valid for small optical bias and induced birefringence [10]), reducing the optical bias magnitude corresponds with reducing the intensity of the local oscillator. Therefore the magnitude of the heterodyne signal (which varies linearly with the induced birefringence) decreases relative to the homodyne signal component (which varies quadratically with the induced birefringence), leading to severe distortions in the observed signal. Fortunately, for equal-magnitude positive and negative optical bias settings, the amplitude and time dependence of this quadratic (and higher order component) signal is identical, whereas the linear signal changes sign. Therefore, subtracting the negative bias signal from the positive bias signal cancels the nonlinear signal components and recovers the enhanced signal that varies linearly with the induced birefringence.

In Fig. 3 we show the difference between positive and negative optical bias traces. The signal distortions are removed, and the resulting signal is directly proportional to the terahertz electric field. In Fig. 3(a) we see a clear increase in signal intensity as the optical bias is reduced. In Fig. 3(b) all the traces are normalized and overlaid, showing that all traces

reproduce the same waveform. This confirms that the signal is enhanced linearly for all optical biases and electric field strength values contained in the trace; this is notable given the large nonlinearities seen in the raw traces in Fig. 2. The small differences observed between traces in Fig. 3(b) are due to slow variations in the terahertz pump intensity from trace to trace.

The theory we developed [10] quantitatively predicts the signal enhancement as a function of optical bias magnitude observed in Fig. 3(a), as well as the signal distortion seen in the raw traces in Fig. 2. For cases 1 and 3, the signal enhancement $g_{P1/VWP}$ in the absence of scattering background is given by

$$g_{P1/VWP}(\Gamma_0) = \frac{1}{\sin \Gamma_0}, \qquad (2)$$

and for case 2, the signal enhancement g_{QWP}, with the same assumption of no scattering background, is given by

$$g_{QWP}(\theta) = \frac{1}{\sin(2\theta)(1 + \cos^2\theta)}, \qquad (3)$$

where $\Gamma_0 = \cot^{-1}[\cot(2\theta)\cos(2\theta)]$ is the QWP optical bias. Figure 4(a) shows the signal enhancement as a function of optical bias. Many (nonzero) values for a variety of time delays from the traces in Fig. 3(a) are divided by the 90° optical bias data at the same delay to give a normalized enhancement (divided by 80° data for the VWP); the selected delays are then
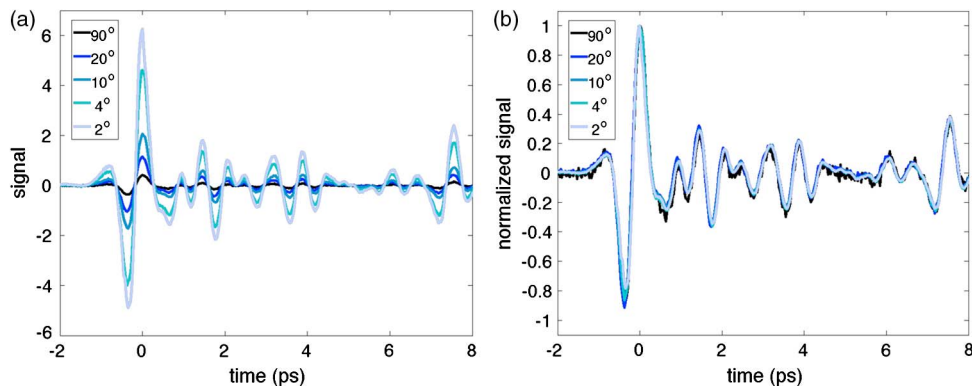

Fig. 3. (a) Difference between the positive and negative optical bias traces from Fig. 2. (b) The same traces as in (a), normalized and overlaid.
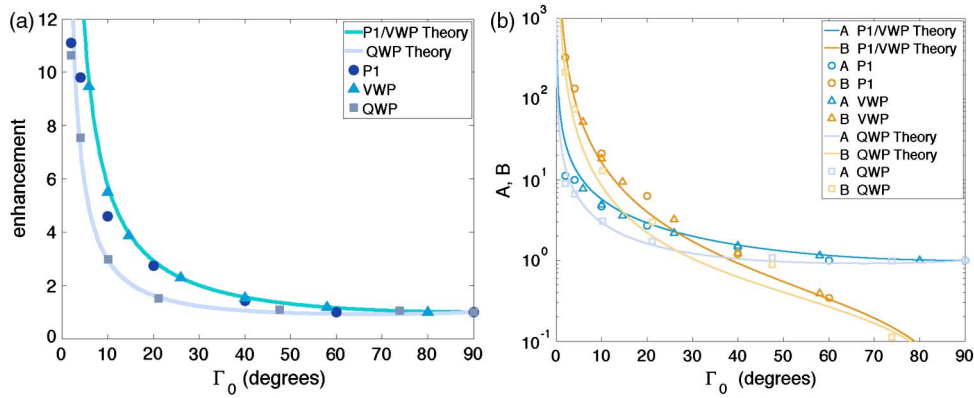
Fig. 4.   (a) Signal enhancement, averaged for many delay times (identical for each trace) and normalized to the 90° optical bias values (the VWP data was normalized to the 80° optical bias value). Circles are for rotating P1 (case 1), squares are for adjusting the VWP (case 3), and triangles are for rotating the QWP (case 2). The solid lines are the theoretical enhancement in the absence of a scattering background ($b_\perp = 0$). (b) Theoretical and fitted values for A and B parameters (respectively, the linear and quadratic raw signal component amplitudes as described in the text). As in (a), circles are for rotating P1, squares are for adjusting the VWP, and triangles are for rotating the QWP.

averaged together to give the points in Fig. 3(b). Circles are for case 1 (rotating P1), triangles are for case 2 (rotating the QWP), and squares are for case 3 (a different phase-retardation set with the VWP). The solid lines are the theoretical enhancements as a function of optical bias from Eqs. (2) and (3). Cases 1 and 3 provide slightly larger enhancement than case 2, and VWP and QWP data show good agreement with the predicted behavior for all measured optical bias magnitudes.

As described in Ref. [10], due to scattered light from imperfections in the EO crystal and other optics, the enhancement will not continually increase as the optical bias is reduced. This departure from ideal behavior is seen clearly in the P1 data [circles in Fig. 3(b)]. For the lowest optical bias data, the ratio of scattered light was nearly 50% more in the P1 data compared to the VWP data, and thus a larger departure from the ideal enhancement was expected. Regardless, roughly an order of magnitude signal enhancement was observed at the lowest optical bias for all three cases.

In Fig. 4(b), we see a comparison between the theoretical distortion and that observed in the raw traces in Fig. 2. In the limit of small terahertz-induced phase retardation Γ_{THz}, the signal can be approximated by the second order polynomial,

$$S = A\Gamma_{\text{THz}} + B\Gamma_{\text{THz}}^2, \qquad (4)$$

where the coefficient A is equal to the enhancement factor g and the coefficient $B = dg^2$, where d is the first-order distortion parameter as defined in Ref. [10]. As described above, in the optical-heterodyne-detection framework, the A signal component that varies linearly with Γ_{THz} is the heterodyne signal and the B signal component is the homodyne signal. In the absence of background scattering, the quadratic signal amplitude coefficient B is given by

$$B_{P1/\text{VWP}}(\Gamma_0) = \frac{g}{2} \cot \Gamma_0 \qquad (5)$$

and

$$B_{\text{QWP}}(\theta) = \frac{\cot^2 2\theta}{2(1 + \cos^2 2\theta)}, \qquad (6)$$

where the QWP optical bias is as above, $\Gamma_0 = \cot^{-1}[\cot(2\theta)\cos(2\theta)]$. In order to compare this prediction with the real signals before subtracting opposite optical bias traces, such as those shown in Fig. 2 for case 1, a fitting routine was employed to calculate the A and B coefficients. For a trace collected for a given optical bias, the entire trace was fit to the form given in Eq. (4) using the 90° optical bias data as the input for Γ_{THz} (or the 80° optical bias trace for the VWP data). The fitted values of A and B were averaged for positive and negative optical bias traces and then plotted in Fig. 4(b) together with the theoretical predictions. We see fairly good agreement between all the points and the theoretical lines. The differences between the fit values and the theoretical lines are possibly due to the noise in the 90° optical bias data used to generate the fits, as well as to neglecting background scattering in the theoretical lines and higher order terms in the fitting function. Note that the amplitude of the quadratic signal component is less when using the QWP (case 2) than using P1 or the VWP (cases 1 and 3) for all optical biases [see the orange solid lines in Fig. 4(b)], but for an equal linear signal enhancement [the blue solid lines in Fig. 4(b)] the corresponding quadratic signal amplitude in the QWP case is always higher than for the same signal enhancement in either the P1 or VWP cases.

As there may be some small error in setting the negative optical bias magnitude to equal the positive bias magnitude, we briefly discuss potential consequences to the subtracted signal in terms of the A and B parameters. If the positive and negative optical bias magnitudes are identical, subtracting the traces doubles the linear A term and cancels out the quadratic B term. If the negative optical bias magnitude is slightly different by an angle $\Delta\Gamma_0$ from the positive setting, some residual quadratic signal will remain in the subtracted signal. The residual quadratic signal amplitude can be calculated as $\Delta B(\Gamma_0, \Delta\Gamma_0) = B(\Gamma_0) - B(-\Gamma_0 + \Delta\Gamma_0)$; it can be neglected if Γ_{THz} is small and if ΔB is small in comparison to the linear signal amplitude A. Using Eqs. (2) and (5) for P1 or a VWP, we plot in Fig. 5 the ratio $\Delta B(\Gamma_0, \Delta\Gamma_0)/2A(\Gamma_0)$ for two deviations in angle ($\Delta\Gamma_0 = 0.05°$ and $0.01°$). We see that the relative quadratic signal strength first increases slowly when reducing the optical bias angle, then quickly becomes significant at small biases. The ratio reaches 10% for optical biases of
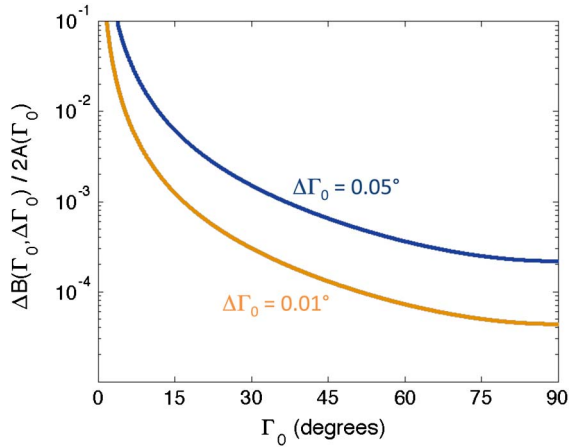
Fig. 5. Ratio $\Delta B(\Gamma_0, \Delta\Gamma_0)/2A(\Gamma_0)$ plotted with errors in the negative optical bias of $\Delta\Gamma_0 = 0.05°$ and $0.01°$ when rotating P1 or using a VWP. The relative quadratic signal magnitude reaches 10% at $3.74°$ and $1.68°$ for $\Delta\Gamma_0 = 0.05°$ and $0.01°$, respectively.

$3.74°$ and $1.68°$ for angle errors of $0.05°$ and $0.01°$, respectively. In the scaled traces in Fig. 2(b), errors on the order of 10% are absent even for the lowest optical bias data, suggesting that we have better than $\pm 0.01°$ accuracy in setting the negative optical bias magnitude equal to the positive optical bias.

Because all three cases give similar maximum signal enhancement, we offer some points to consider when deciding which method to implement. As mentioned above, high-quality polarization optics and EO crystal are essential to high-sensitivity measurements. There may be cost advantages to the P1/QWP cases over the use of a polarizer and VWP, as a compensator is often more expensive than a QWP. If signal enhancement is to be quantified, the VWP we used needs to be calibrated, which may add some uncertainty to the signal gain factor (although this calibration is not needed for all VWPs). When rotating P1, one difficulty may arise depending on the choice of polarizer. Glan-Laser or Glan–Taylor polarizers that are not well aligned may walk the beam and disrupt spatial overlap when rotated. To circumvent this potential problem, we used a linear film polarizer (Thorlabs LPVIS050-MP) with a high extinction ratio ($>10^8$) at the 800 nm probe wavelength that does not change beam pointing when rotated.

Alternatively, the QWP may be rotated without affecting the beam pointing. For pure transient birefringence signals, this method of rotating the QWP is acceptable. But as pointed out in Section 5 of Ref. [10], in the OHD-OKE framework, the signal and local oscillator are not exactly in phase. In the OHD-OKE literature, the distinction is made between detecting polarization rotation induced by birefringence and that induced by dichroism [7–9]. The dichroism signal is $90°$ phase shifted from the birefringence signal, and thus introducing the local oscillator by rotating the QWP can lead to a signal of mixed birefringence and dichroism, whereas rotating P1 (or using a VWP) with the local oscillator at $0°$ or $180°$ allows isolation of the birefringence signal [7–9]. With measurements of free-space terahertz radiation by EO sampling, the signal is by and large pure birefringence, so rotating the QWP does not adversely affect the data interpretation.

Rotating the QWP for signal enhancement also may allow for one small modification to expedite the data collection. As mentioned in Ref. [10], it makes no difference if the QWP is placed before the sample, as in Fig. 1, or after the sample (before P2). A nonpolarizing beam splitter may be placed after the lens with a QWP and analyzer for both beams, allowing one QWP to be set for positive optical bias and the other to be set for the equivalent negative optical bias. Then each resulting perpendicular polarization beam can be sent to one of two photodiodes. Even though this requires two QWPs and two analyzing polarizers, only one trace would need to be collected, and the signal distortions may be removed according to Eq. (44) in Ref. [10]. This may be particularly useful for low-repetition-rate laser systems that require longer acquisition times, and furthermore, it should be compatible with single-shot probing techniques [14,15].

4. CONCLUSIONS

We have demonstrated an experimental procedure showing an order-of-magnitude increase in sensitivity to EO sampling measurements of a free-space terahertz electric field. When working at small optical bias, even large nonlinearities in the signal can be removed by collecting data at positive and negative optical biases and subtracting. Good agreement with the theoretical enhancement from Ref. [10] was observed for traces recorded for a range of optical bias magnitudes.

The signal enhancement described in Ref. [10] and demonstrated here is valid for measurements of any type of transient birefringence. For instance, optical pump OHD-OKE setups have been used to excite and probe Raman active phonon modes through impulsive stimulated Raman scattering [8,16]; optimal enhancement in OHD-OKE measurements can be understood with the framework we have described. Additionally, due to the signal enhancement, this experimental configuration could be an excellent means to probe small transient birefringence signals due to other terahertz-induced excitations. In the case of a mode that is both Raman and IR active, the phonon mode could be resonantly pumped with terahertz, and subsequently probed with an optical transient birefringence probe. This would offer complimentary information to terahertz transmission spectroscopy, because the coherent motion initiated in the sample could be directly observed, rather than measuring the terahertz amplitude missing in the transmitted spectrum. In practice, one often won't need enhancement for accurate measurements of ~100 kV/cm terahertz electric field strengths such as those measured here, but the associated transient birefringence resulting from an excited coherent phonon mode may be much less than that induced by the EO effect in crystals like ZnTe and GaP, and thus for weak signals the signal enhancement offered by working at small optical bias angles would be essential. But as mentioned above, care would need to be taken to separate potential dichroism from birefringence signals.

ACKNOWLEDGMENTS

REFERENCES

1. Q. Wu and X.-C. Zhang, "Ultrafast electro-optic field sensors," Appl. Phys. Lett. **68**, 1604–1606 (1996).
2. Q. Wu and X.-C. Zhang, "7 terahertz broadband GaP electro-optic sensor," Appl. Phys. Lett. **70**, 1784–1786 (1997).
3. P. C. M. Planken, H.-K. Nienhuys, H. J. Bakker, and T. Wenckebach, "Measurement and calculation of the orientation dependence of terahertz pulse detection in ZnTe," J. Opt. Soc. Am. B **18**, 313–317 (2001).
4. N. C. J. van der Valk, T. Wecnkebach, and P. C. M. Planken, "Full mathematical description of electro-optic detection in optically isotropic crystals," J. Opt. Soc. Am. B **21**, 622–631 (2004).
5. E. D. Palik, ed., *Handbook of Optical Constants of Solids* (Academic, 1985), Vol. **V**, Chap. 2, p. 21.
6. Y. Berozashvili, S. Machavariani, A. Natsvlishvili, and A. Chirakadze, "Dispersion of the linear electro-optic coefficients and the non-linear susceptibility in GaP," J. Phys. D **22**, 682–686 (1989).
7. R. Torre, *Time-Resolved Spectropscopy in Complex Liquids: An Experimental Perspective* (Springer, 2007).
8. C. A. Gautier, J. C. Loulergue, and J. Etchpare, "Homodyne and heterodyne impulsive Raman Kerr nonlinearities in crystal: application to E-symmetry polariton modes in PbTiO$_3$," Solid State Commun. **100**, 133–136 (1996).
9. D. McMorrow and W. T. Lotshaw, "Intermolecular dynamics in acetonitrile probed with femtosecond Fourier transform Raman spectroscopy," J. Phys. Chem. **95**, 10395–10406 (1991).
10. F. D. J. Brunner, J. A. Johnson, S. Grübel, A. Ferrer, S. L. Johnson, and T. Feurer, "Distortion-free enhancement of terahertz signals measured by electro-optic sampling. I. Theory," J. Opt. Soc. Am. B **31**, 904–910 (2014).
11. F. D. J. Brunner, O.-P. Kwon, S.-J. Kwon, M. Jazbinšek, A. Schneider, and P. Günter, "A hydrogen-bonded organic nonlinear optical crystal for high-efficiency terahertz generation and detection," Opt. Express **16**, 16496–16508 (2008).
12. C. Ruchert, C. Vicario, and C. P. Hauri, "Scaling submillimeter single-cycle transients toward megavolts per centimeter field strength via optical rectification in the organic crystal OH1," Opt. Lett. **37**, 899–901 (2012).
13. C. A. Werley, S. M. Teo, and K. A. Nelson, "Pulsed laser noise analysis and pump-probe signal detection with a data acquisition card," Rev. Sci. Instrum. **82**, 123108 (2011).
14. N. H. Matlis, G. R. Plateau, J. van Tilborg, and W. P. Leemans, "Single-shot spatiotemporal measurements of ultrashort THz waveforms using temporal electric-field cross correlation," J. Opt. Soc. Am. B **28**, 23–27 (2011).
15. Y. Minami, Y. Hayashi, J. Takeda, and I. Katayama, "Single-shot measurement of a terahertz electric-field waveform using a reflective echelon mirror," Appl. Phys. Lett. **103**, 051103 (2013).
16. Y. Yan and K. A. Nelson, "Impulsive stimulated light scattering. I. General theory," J. Chem. Phys. **87**, 6240–6256 (1987).